Advanced Steel Construction – Vol. 21 No. 5 (2025) 367–379
DOI:10.18057/IJASC.2025.21.5.1

STUDY ON FLEXURAL PERFORMANCE OF NEW THIN-WALLED U-BEAM-WOOD H-SECTION COMBINATION BEAMS

Chang Wu [1, 2], Dong-Dong Ma [1, *], Zhi-Jiang Zhao [1], Ren-Jun Fang [1] and Yie-Gong Xu [1]

[1] *School of Civil Engineering, Lanzhou University of Technology, Lanzhou 730050, China*
[2] *Western Center of Disaster Mitigation in Civil Engineering of Ministry of Education, Lanzhou University of Technology, Lanzhou 730050, China*
** (Corresponding author: E-mail: 3175275739@qq.com)*

ABSTRACT

This study focuses on the analysis of combining the advantages of steel and wood. And then, we propose a new thin-walled H-section steel-wood combination beam, which is connected by a mixture of epoxy resin adhesive and self-tapping screws. In this paper, the bending capacity test is carried out on 7 steel-wood combination beams with the screw spacing, steel profile thickness, web height, and flange board thickness as the influencing factors, and analyze by finite element software modeling. The results show, that the overall performance of the combined beams is good, and the final failure mode of the combined beams is typical bending tensile damage with the tensile cracking of the planks on the tensile side. The change of self-tapping screw spacing on the flange of the combined beam has no obvious influence on the bending load capacity. The increase in the thickness of the flange plank, the thickness of the thin-walled steel section, and the height of the web of the combined beam has a significant increase in the bending load capacity. The adopted finite element model is reasonable and effective, and the calculation results are in good agreement with the test results.

ARTICLE HISTORY

Received: 22 November 2024
Revised: 4 January 2025
Accepted: 8 January 2025

KEYWORDS

Combined steel-wood beams;
Flexural load capacity tests;
Damage mechanisms;
Finite element simulations

1. Introduction

Wood can be recycled many times, which is representative of environmentally reusable building materials. Its processing is convenient and can also be assembled in the field construction. Steel has high strength, good plasticity, and toughness properties. When connecting with different materials or components, it can be connected by bolts, rivets, and other strong and reliable connections. It is a kind of economic, sustainable development of environmentally friendly building materials. Cold-formed thin-walled steel[1-2] is used as a 1.5mm~5mm thin steel plate in the cold state directly bent and processed into a variety of cross-sectional shapes of the steel. However, due to the thin wall thickness, high strength of large cross-sectional openings, and other characteristics, thin-walled steel is prone to instability when subjected to pressure or bending. Steel-wood combination structure combines the good performance of the two, can let them bear the load together, through different ways of combining can play the role of different materials in the structure.

Therefore, scholars at home and abroad began to study the use of wood in combination with steel or other materials to form a combination of members. Shen Yan[3] conducted three sets of tests using three different connections to investigate the full range of behavior of steel beam-column connections. After performing a number of tests, it was found that the variability stems from random changes in geometry and material properties. Guzman[4] had analyzed space lattices with triangular and rectangular cross sections, obtaining a continuous representation model from the energy approach, as well as modeling the lattice as an equivalent property for beams and columns. The results allow us to establish the excellent performance of the equivalent properties obtained for each lattice pattern considered. With the advantage of low computational costs involved in implementation, modeling and processing, a point that deserves more research. Linjie Tian[5] was developed analytical and numerical models for predicting the LTB (The lateral torsional buckling) strength of I-beams arranged by different numbers of lateral braces. And they subjected to two movable concentrated loads during the pre-bending phase. An improved Rayleigh-Ritz method was proposed based on the confinement effect of neighboring beam segments. It was used for parameter selection and LTB strength prediction in the pre-bending stage of steel I-beams, providing a theoretical basis for research in this direction. Haixu Yang[6] studied a new type of cold-formed thin-walled steel and glued laminated timber combination of box girders, the composite beams exhibit higher shear strength than a steel or timber beam.Exploring the effect of parameters on the shear capacity of combined beams, where the shear span ratio has the greatest effect on the shear capacity of combined beams.In the steel skeleton in the form of a box-shaped combination of the cross-sectional shear stiffness does not change much. But shear load carrying capacity than the “I” shaped combination form by 12%. E. McConnell[7], used a series of four-point bending tests that were conducted, under service loads and to failure, found that the stiffness and bending properties of prestressed tendon-wood composite beams were greatly improved compared with pure glued-laminated timber beams, and the effect of load-carrying capacity improvement was significant. Marco Corradi[8], applied in the region where tensile stresses, with significant cost-savings and higher charac teristics in term of “minimum intervention”. The improvement of the bending capacity of timber beams under static loads was reinforced with FRP [9-11]. There was a significant improvement in the bending performance of wooden beams under FRP. It was analyzed that imperfections such as cracks and knots in wood beams can make them deform and crack prematurely during the stressing process. He[12], used a general theoretical model considering the typical tensile failure mode, found that the reinforced glulam beams are featured with relatively ductile bending failure, compared to the brittle tensile failure of the unreinforced ones. Hassanieh[13], empirical formulas and load-slip for corrected orthotropic anisotropic glued timber (CLT)-steel composite nodes were obtained by performing indoor pushover tests on CLT-steel-CLT specimens. Wang[14], proposed an approach to improve the bending capacity of wood beams under static loads through the use of self-tapping screws across the beam inclined and staggered along the longitudinal axis of the beam for steel-wood composite connection members. It was shown that the screws have a significant effect on the shear capacity of the members when driven into them at different angles and that they reduce the resisting stiffness. Chiniforush[15], numerical simulation of long-term performance of steel-wood composite structural beams under sustained loading, the results of parametric studies suggest a creep coefficient of 0.35 for 50-years’ design life of STC beams. Zhao[16], by three groups of four-point bending tests and finite element simulations, increasing the number of hybrid-anchored screws can significantly improved the slip stiffness of the connection interface of STC beams and reduce the slip. Song[17], proposed a wood-steel tube composite beam consisting of wood and cold-formed thin-walled rectangular steel. The experiments showed that the epoxy adhesive connection alone had better deformation capacity and load-carrying capacity compared to the beam connected by a composite of screws and epoxy adhesive.

Li[18] found that for every 200% increase in glued wood section, the flexural capacity of the composite beam increased by 16.08%-20.70%, and for a 50% increase in steel thickness, the flexural capacity of the composite beam increased by 33.73%-37.69%. The overall performance of the H-beam larch composite beam was good. Duan[19], three hot-rolled H-beam-larch composite beams and one pure steel beam were tested for bending capacity, found that bonding wood panels to both sides of the steel beam web could increase the load capacity, and the shape of the member was more reasonable and effective. R[20] three hot-rolled H-beam-larch composite beams and one pure steel beam were tested for bending capacity, showed a "two-hinge" yielding mode for all the specimens considered and found that the bolted connection was lower than the self-tapping screw connection in terms of stiffness and ductility. Chen[21] used a four-point bending test to measure

the bending performance of steel-wood composite I-beams under various connection methods, showed that compared to steel-concrete structures, steel-wood hybrid structures have a good performance in terms of flexural load-carrying capacity. Structures, steel-wood hybrid structures have shorter construction times and good seismic performance.

Duan[22] proposed a kind of combined beam with an I-beam cross-section by bonding wood plates at the upper and lower flanges of H-shaped steel, which proved that the combined effect of steel-wood combined beam was significant, the overall synergistic stress performance was good, and the final damage mode of the member was the fracture of wood at the lower flange. Liu Degui[23] designed the thin-walled H-shaped steel wrapped around the wood plate combination beam, compared with pure wood beam combination beam ductility, section stiffness, and bending performance in the presence of steel are greatly increased.

Based on domestic and foreign scholars[24-25] for steel-wood combination beam cross-section combination form, a combination of connection and force performance[26-29], and other research. This paper proposes two back-to-back and stands U-beams as the skeleton, in the middle of the U-beam, a plank, steel plate, and plank using epoxy resin AB glue[30-32] to combine the initial formation of the steel—wood combination body. Next, in the formation of the combination of the skeleton flange on the superior and lower sides. Respectively, with the structural bonding agent two wooden plates are bonded to form an H-shaped cross-section. Then self-tapping screws and bolts are driven into the flange and web respectively to form a steel-wood combination beam as shown in Fig. 1. To verify the reasonableness of the designed combined beam, the three-point bending test is carried out on the combined beam. The parameters such as self-tapping screw spacing, profile thickness, web height, and flange board thickness of the combined beam are used to study the flexural load capacity of the combined beam. The corresponding finite element simulation analysis is carried out to verify its reasonableness by comparing numerical simulation and test.

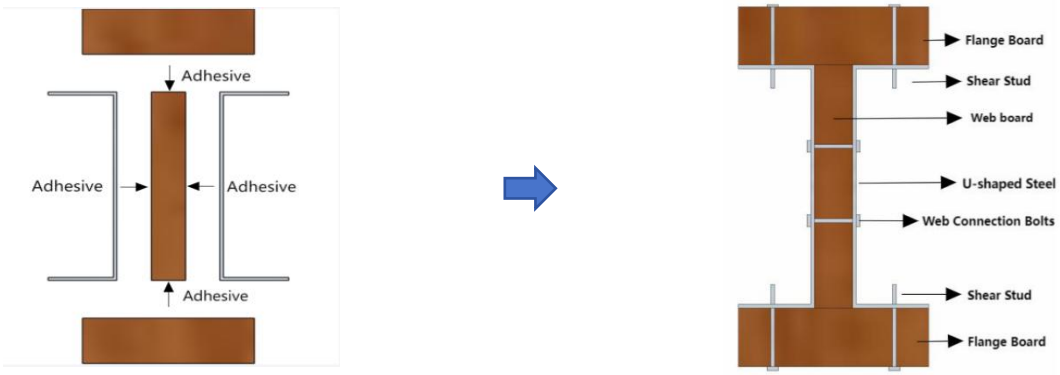

(a) Cross-section of steel-wood combination beam

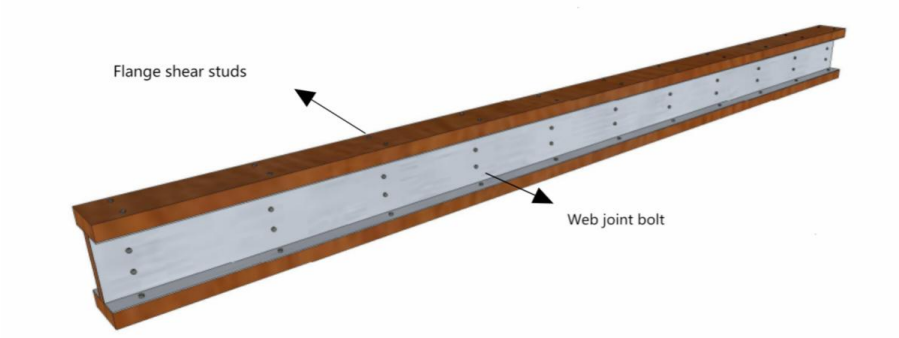

(b) Three-dimensional drawing of steel-wood combination beam

Fig. 1 Steel-wood combination beam

2. Test overview

2.1. Specimen design

This test will design 7 thin-walled H-shaped steel-wood combination beams (Specific parameters are shown in Table 1) for bending capacity test, the test to the combination of beam cross-section dimensions like width and height, shear connectors spacing, and the combination of beam steel plate thickness as a parameter to start. Seven thin-walled H-shaped steel-wood combination beam specimens numbered L-1 to L-7. The combination of beams are 2.5m in length and the calculation of the span of 2.3m. Study the damage process, damage characteristics, and failure modes of the combined beams.

Table 1
Specific parameters of thin-walled H-shaped steel-wood combination beams

Serial number	Plate thickness(mm)	Steel thickness(mm)	Section dimensions of steel	Pitch of	Combined beam cross-section
L-1	30	1.5	30×125×30	240	80×185×80
L-2	30	1.5	40×125×40	240	100×185×100
L-3	30	1.5	40×125×40	180	100×185×100
L-4	30	1.5	40×125×40	120	100×185×100
L-5	30	2.0	40×125×40	120	100×185×100
L-6	40	1.5	40×125×40	120	100×205×100
L-7	30	1.5	40×165×40	120	100×225×100

Note: The thickness of the test beam web planks are 20mm, the axial spacing of the web connecting bolts are 240mm and the height direction spacing is half of the height of the web; the cross-section size of the steel section is the size of the outer edge of the U-type steel plate.

2.2. Specimen production

Timber: Choose Douglas fir timber, the surface of the timber is flat, and no prominent defects or other phenomena.Steel: use Q 235 thin-walled steel, through cold processing into the required U-shaped steel size. Binder (two-component epoxy resin glue): E44 two-component AB epoxy resin glue is used. Connectors: bolts with a diameter of 5mm and a length of 35mm (M5×35mm), countersunk head self-tapping screws with a diameter of 5mm and a length of 50mm (M5×50mm). Step 1: Make the timber boards and galvanized thin-walled steel plates needed for the combination beam for the test to the required size. Step 2: The surfaces of the timber and thin-walled steel profiles to be sanded were leveled and smoothed. Then wipe off the dust from the surface of the wood. Step 3: Apply the structural adhesive on the surface of steel and wood and maintain the combined beam specimen. Step 4: After the maintenance retains a certain strength, in the combination of beams on the upper and lower flange according to the design spacing into the self-tapping screws, in the web according to the design spacing holes and tighten the bolts. At this point, the whole steel-wood combination beam specimen production is completed. The complete specimen of the combined beam is shown in Fig. 2.

Fig. 2 Finished steel-wood combination beam member

2.3. Mechanical properties test of epoxy resin adhesive

2.3.1. Determination of modulus of elasticity, tensile strength

The modulus of elasticity and tensile strength of the epoxy resin AB adhesive material used in the test were determined as follows. The dimensions were designed in accordance with the General Principles of Test Methods for Properties of Resin Casting Bodies (GB/T 2567-2008) and Test Methods for Tensile Properties of Resin Casting Bodies (GB/T 2568-2008). The production requires mixing the two at 1:1 and pouring them into the mold when uncured. At room temperature 25°, leave for 2 days to fully cure, during which time it should not be moved.

The tensile strength of epoxy resin AB adhesive is calculated according to eq. 1:

$$\sigma_t = \frac{F}{bh} \quad (1)$$

Where, σ_t is tensile strength of epoxy resin AB adhesive,units is MPa; F is destructive load, units is kN; b is width of the specimen, units is mm; h is thickness of the specimen, units is mm.

The modulus of elasticity of the epoxy resin AB adhesive is calculated by eq. 2:

$$E = \frac{Fl}{A\Delta l} \quad (2)$$

Where, E is modulus of elasticity of epoxy resin AB adhesive,units is MPa; F is destructive load, units is kN; A is cross-sectional area of the specimen, units is mm^2; l is original length of the specimen, units is mm; Δl is elongation of the specimen, units is mm.

As shown in Table 2, the average tensile strength of the epoxy resin adhesive was calculated to be 14.99 MPa and the modulus of elasticity was 1110 MPa.

Table 2
Test results of epoxy resin adhesive specimens

Specimen Number	Thickness (mm)	Breaking Load (kN)	Tensile Strength (MPa)	Average Tensile Strength (MPa)	Modulus Of Elasticity (MPa)
1	5.1	0.76	15.21		
2	4.9	0.55	11.22		
3	4.8	0.64	13.33		
4	4.6	0.93	20.22		
5	4.7	0.70	14.89	14.99	1110
6	5.0	0.75	15.00		
7	5.1	0.73	14.31		
8	4.9	0.72	14.69		
9	4.8	0.77	16.04		

2.3.2. Epoxy resin adhesive load-displacement curve

The load-displacement curve relationship of the epoxy resin adhesive specimen is shown in Fig. 3. From the load-displacement curve, it can be seen that the curve shows a linear relationship. The damage of the epoxy resin specimen is sudden brittle damage and the yield point before fracture is not obvious. After fracture, the bearing capacity will drop to 0. From the test, it can be seen that the epoxy resin adhesive belongs to the brittle material.

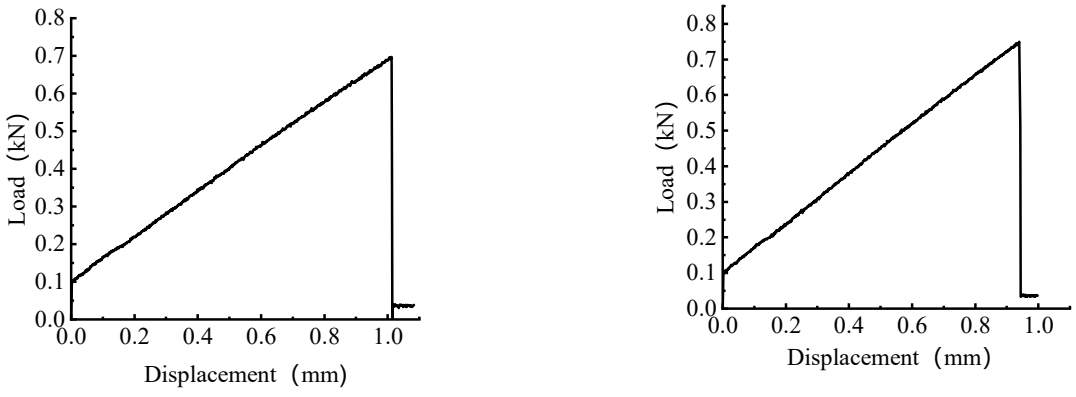

（a） （b）

Fig. 3 Load-displacement graphs

2.4. Determination of material mechanical properties

2.4.1. Adjustment of wood parameters considering defects

Wood is an anisotropic material, and defects are not obvious in the small sizes of specimens used in wood properties tests, but are inevitable in full-size specimens. Timber material defects will produce uncertainty in the use of structural safety, the need to reduce the timber parameters. The main factors affecting the discount factor are natural defects in the specimen (knots, insects, cracks, etc.), long-term loading, drying defects (drying inhomogeneity), dimensional effects. Reduction factor reference Eq. 3：

$$K_Q = K_{Q1}K_{Q2}K_{Q3}K_{Q4} \quad (3)$$

Where, $K_{Q1}$is influence coefficient of natural defects in wood; K_{Q2} is influence coefficient of drying defects of wood; K_{Q3} is influence coefficient of long-term loading strength of wood; K_{Q4} is influence coefficient of dimensions of wood. The reduction coefficient for different impact factors are shown in the table 3.

Table 3
Reduction coefficient for different impact factors

Stress State Of Wood	Compressive Strength Of Smooth Grain	Parallel Grain Tensile Strength	Bending Strength
Effects Of Natural Wood Defects K_{Q1}	0.66	0.80	0.75
Effects Of Wood Drying Defects K_{Q2}	0.90	——	0.85
Long-Term Load Strength Effects K_{Q3}	1.0	1.0	1.0
Wood Size Effects K_{Q4}	0.75	——	0.89
Discount Factor K_Q	0.446	0.80	0.567

Note: This factor is 1.0, because the wood used in this test was new and not subjected to long-term loading.

Due to the wood itself defects and volume effect will have an impact on the mechanical properties, wood damage belongs to the empirical judgment, the discount factor is taken as 0.6 for discounting. The test results of wood material properties after discounting are shown in Table 4:

Table 4
Mechanical parameters of wood

Wood	Parallel-To-Grain Compressive Strength /MPa	Tensile Strength Parallel to Grain /MPa	Flexure Strength /MPa	Elastic Modulus /MPa
Douglas Fir	34.18	50.96	36.08	10290

2.4.2. Mechanical parameters of thin-walled steel

The ultimate strength and yield strength of the specimen are calculated as shown in eq. 4. Where, σ is yield strength and ultimate strength of the specimen, units is MPa; F yield load and ultimate load of the specimen, units is kN; A is section area of the specimen, units is mm^2 .

$$\sigma = \frac{F}{A} \quad (4)$$

The modulus of elasticity for the design is shown in equ. 5. Where, E is modulus of elasticity of the specimen, units is MPa; F is the specimen is subjected to axial tension, units is kN; l is original scale distance of the specimen, units is mm; A is the cross-sectional area of the specimen, units is; Δl is elongation of the specimen, units is mm.

$$E = \frac{Fl}{A\Delta l} \quad (5)$$

According to the relevant data of the specimen automatically collected by the computer, the load-displacement curve of the specimen is drawn, as shown in Fig.4 and Fig.5. Then the obtained data are substituted into equ. 4 to calculate the strength of the specimen. The relevant data are substituted into equ. 5 to calculate the modulus of elasticity of the specimen. The calculation results are shown in Table 5.

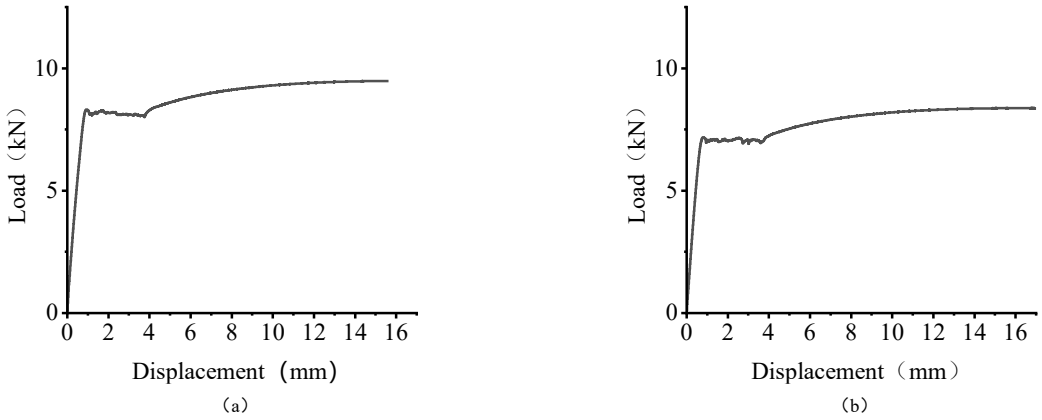

Fig. 4 Load-displacement curve of 1.5mm thick Q235 thin-walled steel section

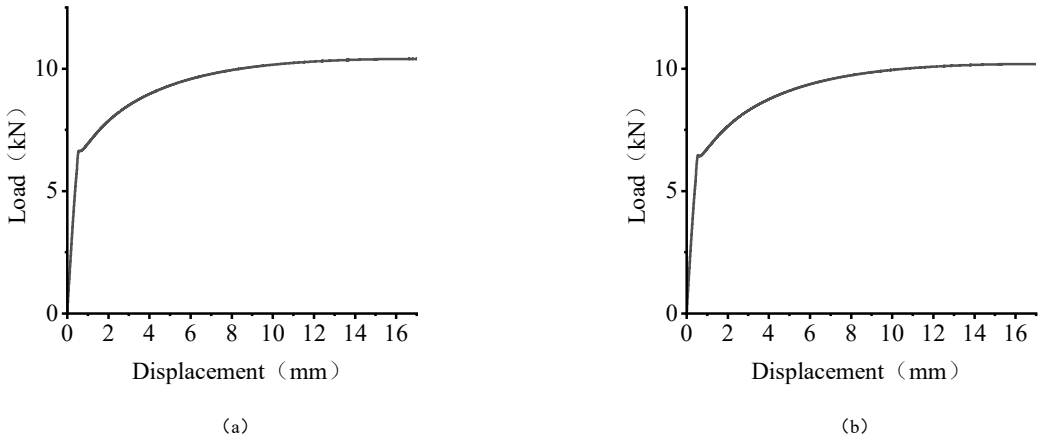

Fig. 5 Load-displacement curve of 2mm thick Q235 thin-walled steel section

Table 5
Mechanical parameters of thin-walled steel

Thicknesses（mm）	Serial Number	Yield Strength（MPa）	Average Yield Strength（MPa）	Ultimate Yensile Strength（MPa）	Average Limit Tensile Strength（MPa）	Modulus Of Elasticity（MPa）
1.5	1	278.67	272.00	318.24	311.64	2.03×10^5
1.5	2	283.00		321.16		
1.5	3	289.33		331.34		
1.5	4	265.33		303.09		
1.5	5	277.00		316.12		
1.5	6	238.67		279.86		
2	1	253.06	256.85	346.62	360.15	1.99×10^5
2	2	260.69		365.50		
2	3	254.87		357.45		
2	4	260.01		365.31		
2	5	247.43		361.34		
2	6	265.02		364.66		

Materiality test data, the average yield strength of Q235 steel 1.5mm thick is 272.00 MPa, the average yield strength of 2mm thick steel is 256.85 MPa. 1.5mm thick average ultimate tensile strength is 311.64 MPa, the average ultimate tensile strength of 2mm thick is 360.15 MPa. The average elasticity modulus is $\mathbf{2.03\times10^5}$ MPa.

2.5. Test loading and determination

The thin-walled H-shaped steel-wood combination beam test belongs to the static loading test, and the bending loading test is performed on the supported beam specimen. The distribution beam support is 350mm in the span of the test beam. The combined beam test was carried out by displacement loading at a 1 mm/min speed. After loading a grade load, it was necessary to allow the load to act on the combined beam for about 3-5 minutes. Then the next load application after the value on the collector was stabilized, and the data collection was done by computer. However, it was necessary to record the deformation state and the development of cracks in the test beams under different loads. During the loading process, pressure transducers are used to determine the load values, and displacement gauges are arranged in the span, crotch, and support of the combined beam to determine the vertical displacement of the beam. The load, displacement, and strain measurement points of the mid-span section are shown in Fig. 6. The combined beam test's loading program is divided into preloading and formal loading.

The devices and tools to be used in the combined beam test include: model YAW-2000 static hydraulic loading device to apply load to the member, model BZ1403 load cell to collect the load applied to the specimen, model 5G106 displacement transducer to collect the vertical deflection of the member, model DH3816N static collection system to collect the signal and output the data through the computer, computer to process the data, model 120-5AA and 120-3AA strain gauges, rulers, supports, reaction frame devices and so on. data, Model 120-5AA and 120-3AA strain gauges, rulers, supports, and reaction frame devices.

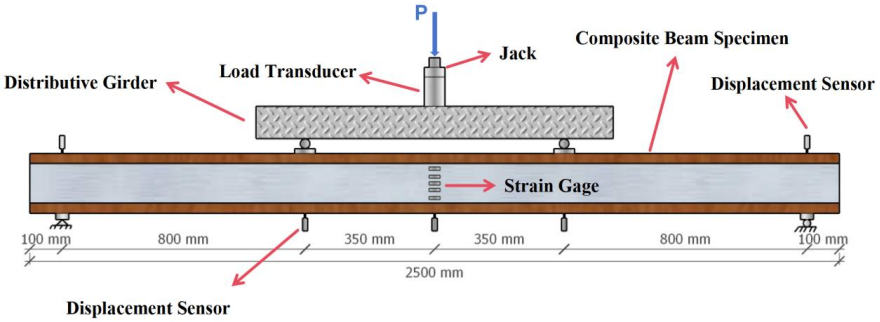

(a)Front elevation loading schematic

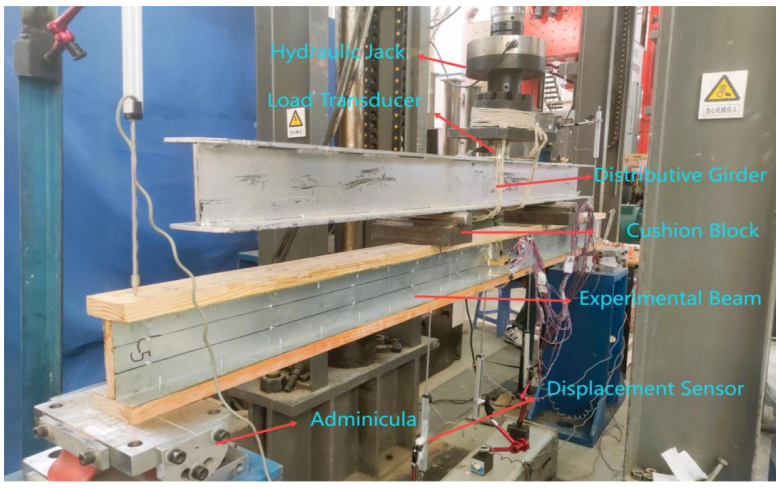

(b) Side elevation loading diagram

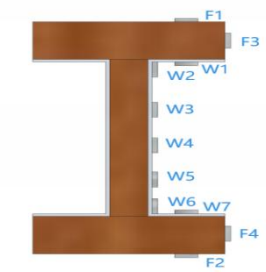

(c) Strain gauge arrangement

Fig. 6 Bending loading diagram of a combined beam

3. Test loading and damage process description

The damage process and damage form of the seven combined beams are similar. All of them are cracked by the structural adhesive between the steel and wood interface at the flange in the elastic stage. To the buckling of thin-walled steel at the flange in the elastic-plastic stage. Then the final destruction of wood at the lower flange to reach the destructive load of the damage process of cracking. The final damage pattern of the combined beam is a typical bending tensile damage. In this section, typical L-5 and L-6 specimens are selected as research objects to analyze the test phenomena.

3.1. L-5 combined beam

L-5 steel-wood beam specimen: Steel thickness specification is 2.0mm, the whole combination of beam cross-section dimensions of 100mm × 185mm × 100mm (width × height × width), and the wing self-tapping screws spacing is 120mm. The web bolts along the height of the web plate, three equal parts of the web plate along the length of the beam spacing of 240mm, the combination of the beam total length of 2500mm.

L-5 combination beam loading early, steel and wood are in the elastic stage. When the load increased to 17kN, the combination of beams occasionally issued a "click" the slight sound, observed and found that the epoxy resin adhesive was not coated with a uniform cracking sound. With the increase in the load to 30 ~ 35kN, the occasional slight sound changes into a crunchy sound and becomes Intensive and increasingly large. Considering due to the force develops into large combined beam steel-wood connection glue cracking in large areas as shown in Fig. 7(a). When the load reaches 48kN, the combination of beams that appeared to the naked eye can be observed in the test phenomenon, spanning the upper and lower edge of the self-tapping screws by the shear tilt as shown in Fig. 7(b). The right side of the centralized loading point of the pressurized side of the thin-walled steel wing edge flexures outward bulge in the concentration of the loading point. Also accompanied by the pressurized area of the plank pressure deformation, planks, and steel sections have a greater separation. Load continues to increase to 54 ~ 63kN, the combination of beams spanning the three-point centralized load at the tensile side of the edge of the plank due to defects in its wood joints, first produced small cracks and then issued a "boom" sound, through the wood joints appear large cracks, and cracks along the beam width and length direction continue to extend, widening the formation of longer split cracks and transverse cracks as shown in Fig. 7(c) and Fig. 7(d). The transverse cracks are shown in Fig. 7(c) and Fig. 7(d). At this time, the load of the combined beam is no longer increased but can still withstand a certain load, and the damage test of the combined beam is declared to be finished.

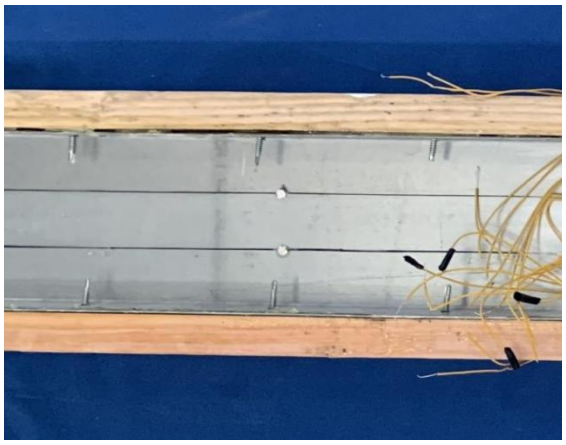

(a) Adhesive mass cracking observed at the L-5 beam steel-to-wood connection

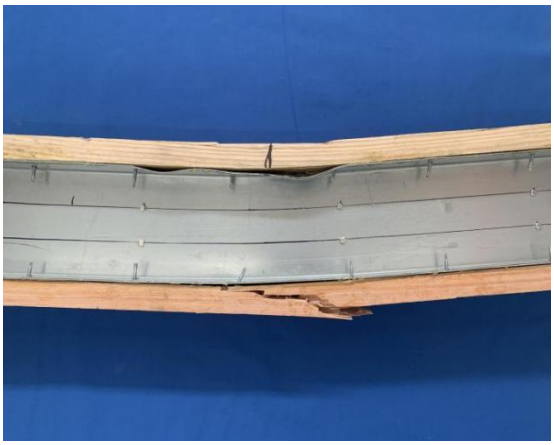

(b) Flange damage in the tensile zone of the L-5 beam and large separation of the planks and sections were observed

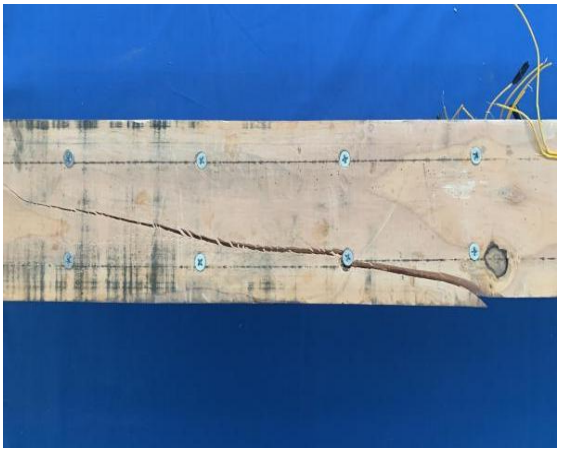

(c) Oblique shear damage of planks between self-tapping screws observed at L-5 beam webs

(d) Further destruction of the planks between the self-tapping screws along the smooth grain observed at the web of the L-5 beams

Fig. 7 L-5 Beam Failure Phenomenon

3.2. L-6 combined beam

L-6 steel-wood beam specimen: Steel thickness specification is 1.5mm, the whole combination of beam cross-section dimensions of 100mm × 205mm × 100mm (width × height × width). The wing self-tapping screw spacing is 120mm, the web bolts along the height of the web plate, three equal parts of the web plate along the length of the beam spacing of 240mm, and the combination of the beam total length of 2500mm.

L-6 combination beam loading initial, steel and wood are in the elastic phase of the common force. When the load increased to 33 ~ 45kN, the combination of beams occasionally issued a "click" of the slight crunching sound and no traces of destruction. After observing the combination of beams for the steel and wood connection of the epoxy resin adhesive cracking ringing sound.With the increase in the load to 55kN, the combination of beams with the increase of load to 55kN. The combined beam made a continuous crunching sound and got bigger and bigger. At this time, due to the consideration of the force becomes a big combined beam steel-wood connection at the adhesive film layer peeling as shown in Fig. 8 (a). When the

load reached 72kN, the combined beam appeared obvious naked eye as observed in the test phenomenon. The upper and lower flange of the span of the self-tapping screws tilted in the shear. The middle of the span and the two concentrations of force loading point of the compression side of the adhesive layer peeling of thin-walled steel flanges in many places to the outward projection of the yielding of the flange as shown in Fig. 8 (b). Fig. 8 (b) showed that the three-point centralized loading point is also accompanied by the section steel web buckling outward buckling bulge as shown in Fig. 8 (c). Load continues to increase to 88kN, the combination of beams on the right side of the loading point of the tensile side of the flange planks issued a "booming" loud sound, and crack along the width of the beam continues to extend. After widening to form a through crack, the crack extends along the length direction as shown in Fig. 8 (d). At this point, the load of the combined beam is no longer increased but still able to withstand a certain load. And the damage test of the combined beam is declared to be over.

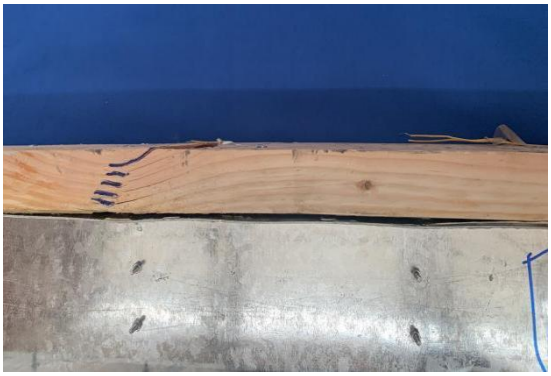

(a) Peeling of adhesive film layer observed at L-6 beams

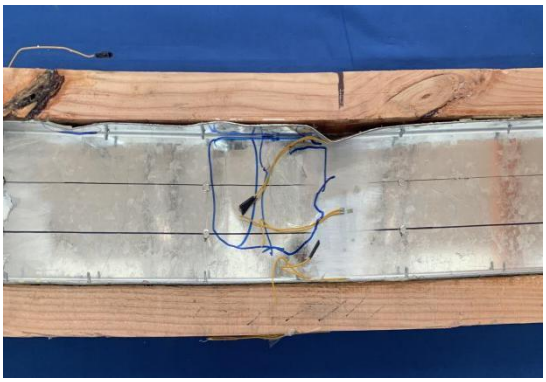

(b) Buckling of the profile flange observed in the L-6 beam compression zone

(c) Buckling of the section web observed at the L-6 beam

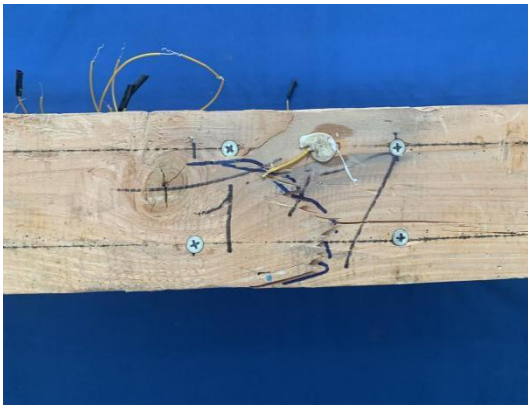

(d) Cracking of planks along the width observed on the tension side of L-6 beams

Fig. 8 L-6 beam failure phenomenon

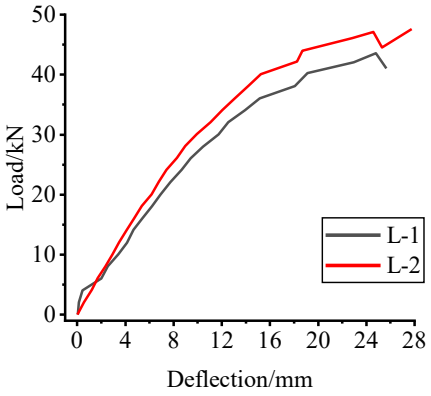

Fig. 9 Comparison of load-deflection curves

4. Results and analysis of test influencing factors

4.1. Influence of cross-section change of combined beam

4.1.1. Influence of flange width of combined beams

Member L-1 combined beam cross-section size of 80mm × 185mm × 80mm, L-2 combined beam cross-section size of 100mm × 185mm × 100mm. L-2 combined beam compared to the L-1 combined beam in other conditions are the same under the premise of the beam width changed to 100mm.

As shown in Fig. 9, by comparing the effect of different flange widths on the flexural capacity of the combined beams. From the load-deflection curve, it can be seen that when the flange width of the combined beams is changed from 80mm to 100mm. The slope of the load-deflection curve of the combined beams changes similarly to the flexural capacity from 43.57kN to 47.08kN. And the maximum flexural capacity is increased by 8.06%. With the increase in the width of the combined beams, the maximum flexural capacity is also increased, and the maximum bending capacity is increased. With the gradual increase of the flange width of the combined beam, the maximum bending capacity also increases but the increase is not large. So the flange width of the combined beam has a small effect on the bending capacity.

4.1.2. Influence of section height of combined beams

Component L-4 combination beam selection of steel section size 40mm × 125mm × 40mm flange plank thickness of 30mm. L-6 composite beam selection of steel section size 40mm × 125mm × 40mm flange plank thickness of 40mm. L-7 composite beam selection of steel section size 40mm × 165mm × 40mm flange plank thickness of 30mm. Combination beam L-4 and composite beam L-6 are compared for the composite beam section height from 185mm to 205mm. Combination beam L-4 and combination beam L-6 for the combination beam section height from 185mm to 205mm. Combination beam L-4 and composite beam L-6 for the composite beam section height from 185mm to 205mm. L-4 compared with the combination beam L-6 for the flange plank thickness changes in the combination beam section height from 185mm to 205mm. Combination beam L-4 compared with the built-up beam L-7 for the steel section size changes in the composite beam section height from 185mm to 225mm.

By comparing the effect of different section heights on the flexural load capacity of the combined beams, as shown in Fig. 10. Through the load-deflection the curve can be seen that the flexural load capacity of the

combined beams L-4 compared with the combined beams L-6 increased from 57.23kN to 89.13kN. The maximum flexural load capacity was increased by 55.74%. The flexural load capacity of the combined beams L-4 compared with the combined beams L-7 increased from 57.23kN to 83.34kN, the maximum bending capacity increased by 45.63%. The slope of the load-deflection curve of the two groups of specimens is almost the same at the beginning of loading. However, with the increase of the load, the stiffness of the specimen of the combined beam L-4 reaches the yielding load. And the slope of the curve starts to degrade and tends to flatten. In summary, due to the different heights of the combined beam section, the corresponding maximum flexural load capacity is different. Combined beam L-6 and combined beam L-7 for the specimen flexural load capacity increase are more obvious. Specimen L-6 and specimen L-7 damage process is similar. They are with the increase in load combination of the beam across the upper edge of the beam began to flex after the lower edge of the timber tensile rupture. But specimen L-6 than the corresponding cracking load L-7 is larger. However, the cracking load of specimen L-6 is larger than that of L-7. From the perspective of the overall load deflection of the specimen and the amount of steel used. It is relatively optimal to choose the combination of specimen L-6 and the load deflection of the combined beam.

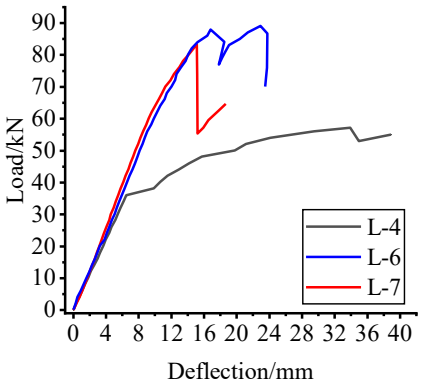

Fig. 10 Comparison of load-deflection curves

4.2. Combination of beams nail spacing change effect

Combined beam L-2, L-3, and L-4 cross-section dimensions are 100mm × 185mm × 100mm. In the case of other conditions are the same combination of the upper and lower flange of the beam into the self-tapping screw spacing is different, respectively, for 240mm, 180mm, and 120mm.

By comparing the effect of different self-tapping screw spacing on the flexural load capacity of the combined beam, as shown in Fig. 11. Combined beam L-2 flexural load capacity of 47.08kN, combined beam L-3 flexural load capacity of 52.19kN, combined beam L-4 flexural load capacity of 57.23kN. Combined beam L-3 than the maximum bending capacity of the L-2 increased by 10.08%. Combined beam L-4 than the maximum bending capacity of the L-3 increased by 10.08%, combined beam L-4 than the maximum bending capacity of the L-2 increased by 10.08%, combined beam L-4 than L-3 increased by 10.08%, combined beam L-4 than L-4 increased by 10.08%, combined beam L-4 than L-3 increased by 10.08%. 3. The maximum bending capacity of the combined beam L-3 was increased by 10.08%, and the maximum bending capacity of the combined beam L-4 was increased by 9.7%. From the specimen load-deflection curves, the overall load deformation of the three groups of specimens was similar. The change in the spacing of the self-tapping screws increased the bending capacity of the combined beam by a small amount. In summary, with the increase of load, the tapping screw spacing decreases, and the phenomenon of tapping screw shear damage gradually increases, which indicates that the interface shear force borne by the tapping screw increases. The combination of adhesive and shear-resistant connection of tapping screws is gradually reflected.

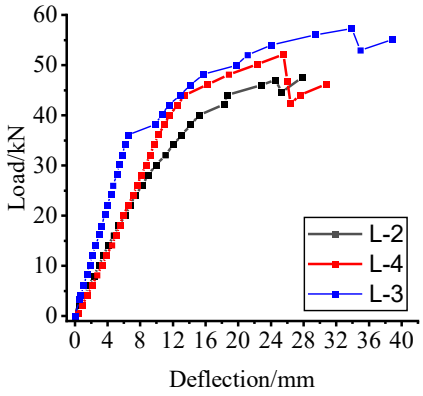

Fig. 11 Comparison of load-deflection curves

4.3. Influence of beam thickness

Combined beam L-4 and combined beam L-5 cross-section size of 80mm × 185mm × 80mm. The difference is that the combined beam L-4 selection of thin-walled steel thickness of 1.5mm. Combined beam L-5 selection of thin-walled steel thickness of 2mm and other conditions are the same.

As shown in Fig. 12, after comparing the steel-wood beam in the steel thickness of the different steel on the steel-wood beam bending capacity. When L-4 combined beams and L-5 combined beams are compared, the degree of thinness of the steel is thickened from the specification of 1.5mm to the degree of thinness of the steel 2mm specification. The bending capacity of L-5 steel-wood beams rises from 57.23kN of L-4 steel-wood beams to 64.09kN, and the peak load of the steel-wood beam specimens rises by about 12%. From the load-deflection curve and test phenomena, the beginning of the loading of the two groups of specimens' load deflection was linear growth. With the increase in load, adhesive peeling gradually increased after the combination of beams L-4 first reached the slope of the yield curve. With the increase in the thickness of the steel, the combination of beams compressed flange compression curvature phenomenon gradually became less obvious, which indicates that increasing the thickness of thin-walled steel can reduce the combination of beams thin-walled steel compression buckling generation. The damage phenomenon is also different when the bearing capacity is reduced. Through the above analysis, it can be seen that the steel thickness specification in the steel-wood beam specimen has a certain degree of influence on the peak load-carrying capacity of the steel-wood beam specimen. When the steel thickness specification of the steel-wood beam specimen is increased from 1.5 mm to 2 mm. The peak load carrying capacity of the steel-wood beam specimen is proportional to the thickness of the steel and the increase in peak load is not significant. However, the overall performance exhibited by the combined beam L-5 is better than that of the combined beam L-4. Therefore, it can be seen from the experimental analysis that the steel thickness specification of 2 mm in the steel-wood beam specimens is better for the overall performance of the steel-wood combination beam.

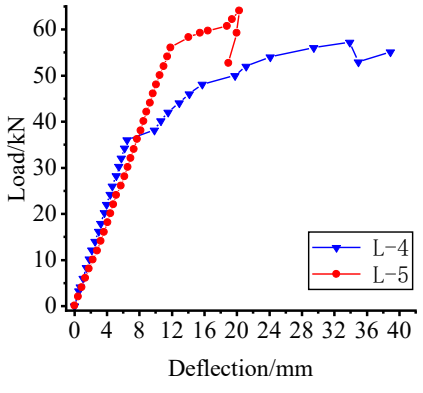

Fig. 12 Comparison of load-deflection curves

Yield point was a key factor in the design and research of engineering structures, and also a key factor in the measurement of structural ductility. Based on the method of P. Feng[33] for the definition of yield point. This

paper adopted the energy equivalent area method for the definition of yield displacement to determine the yield load P_y, the yield displacement Δ_y, and the ultimate load P_u, the ultimate displacement Δ_u are taken from the specimen to reach the peak load in the falling section of the curve with a load of 85% of the maximum load and the displacement value corresponding to this load (Fig. 13). The displacement value corresponding to this load (Fig. 13), and its deformation index ductility coefficient μ is calculated by using eq.6. Table 6 gives the mechanical properties of the combined beams from the test and calculation.

$$\mu = \frac{\Delta_u}{\Delta_y} \tag{6}$$

Where, Δ_u is ultimate displacement of the specimen; Δ_y is yield displacement of the specimen.

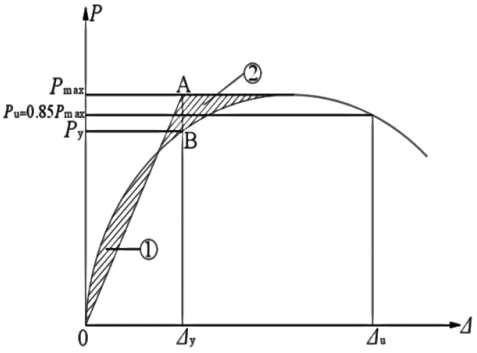

Fig. 13 Equal energy method

Table 6
Mechanical properties of combined beams

Specimen Number	Yield Load		Ultimate Load		Ductility Factor μ
	Py/kN	Δ_y/mm	Pu/kN	Δ u/mm	
L-1	34.06	13.93	41.04	25.67	1.84
L-2	40.07	15.23	44.51	25.28	1.66
L-3	44.05	13.44	42.29	26.43	1.97
L-4	48.01	15.73	52.97	34.96	2.22
L-5	56.16	11.86	52.67	18.98	1.60
L-6	72.18	12.47	70.04	23.51	1.89
L-7	62.08	9.57	55.32	15.21	1.59

From Table 6, it can be seen that the ductility coefficient of L-4 combination beam is the largest, and the ductility is better. The ductility coefficient of L-7 combination beam is the smallest. As a whole, all the steel-wood combination beam specimens have better ductility under bending.

According to the load-displacement relationship curves of thin-walled H-section steel-wood combination beams. It can be seen that all the combination beams are in the elastic stage of the load-displacement curves. It can be assumed that the thin-walled H-section steel-wood combination beams are in the elastic stress stage under the limit state of normal use. Therefore, based on the deflection calculation equation for simply supported beams, the deflection calculation equation for thin-walled H-shaped cross-section steel-wood combination test beams can be given. Substituting the sectional flexural stiffness into the mid-span deflection calculation equation for single-span simply supported beams yields eq. 7:

$$f = \beta_s \frac{FaL^2}{48EI}\left(3 - 4\alpha^2\right) \tag{7}$$

Where: f is Beam mid-span deflection; β_s is deformation development factor; F is value of elastic phase load; a is distance of the point of action of the concentrated force from the support; EI is total stiffness of the combined beam section; L is span of the combined beam; $\alpha = a/L$.

As the main bending load-bearing member in the building structure, the deformation development in the span of the beam needs to meet the limit values specified in the code under the normal use of the limit state when designing. In order to ensure the safety performance of the structure in use. In this paper, steel-wood combination beams should also meet the requirements. According to the relevant provisions of the Code for the Design of Steel Structures (GB 50017-2017)[34] and the Code for the Design of Wood Structures (GB/T 50005-2017)[35]. The combined beam specimens in the normal range of use, the control of deflection of the bending member of the maximum allowable deflection of L/250. 7 steel - wood combined beam specimens are 2.5 meters in length after removing the spacing of the supports, the length is 2.3 meters. The total length of the 7 steel-wood beam specimens is 2.5 meters after removing the spacing between the supports. The length is 2.3 meters, which can be calculated by the formula of the specification to obtain the deflection limit value corresponding to the limit state of normal use of the 7 steel-wood beam specimens as 9.2 mm. The 9.2 mm is substituted into the eq. 7 to calculate the 7 steel-wood beam specimens in the deflection of the specified value of 9.2 mm, when the corresponding loading force for the. The test deflections corresponding to the normal service limit states were found in the load-deflection curves of each specimen. Comparison of the theoretical and experimental values of the deflection of the combined beam under normal use limit state are analyzed as shown in Table 7. The error is within the permissible range and the theoretical calculated value is conservative enough to meet the needs of engineering use.

Table 7
Comparison of theoretical and experimental values of normal service limit state deflection

Specimen Number	Theoretical Deflection (mm)	Test deflection (mm)	Theoretical Deflection/ Test Deflection
L-1	9.20	8.65	1.06
L-2	9.20	9.67	0.95
L-3	9.20	9.11	1.01
L-4	9.20	9.04	1.02
L-5	9.20	8.85	1.04
L-6	9.20	8.16	1.13
L-7	9.20	8.01	1.15

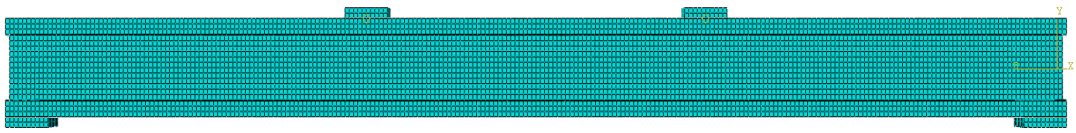

Fig. 14 Grid division

5. Finite element analysis

5.1. Establishment of finite element model

In the finite element modeling, the required two material parts as well as other components. They are established as solid models, and the 8-node hexahedral linear reduced integral C3D8R unit is selected as the unit. Among them, a simplified isotropic ideal elastic-plastic trilinear model is used for the steel principal structure. The anisotropic simulation of wood in the elastic and plastic phases is realized by using the "engineering constants" and Hill's yield criterion of the finite element software, respectively. The mesh size of the cells is 10 mm, and the cell division of the model is shown in Fig. 10. The loading mode is consistent with the experimental loading. The boundary conditions are consistent with the experimental boundary conditions, simply supported on one side and hinged on the other side.

Table 8
Finite element coordinate system and wood orthogonal triaxial correspondence

Input Value	Representative Value	Physical Meaning
E_1	E_L	Longitudinal modulus of elasticity of the smooth grain
E_2	E_R	Radial modulus of elasticity of cross-grain
E_3	E_T	Transverse tangential modulus of elasticity
υ_{12}	υ_{TL}	Transverse radial principal Poisson's ratio
υ_{13}	υ_{LR}	Transverse tangential principal Poisson's ratio
υ_{23}	υ_{RT}	
G_{12}	G_{LT}	Shear modulus on combined longitudinal and tangential surfaces
G_{13}	G_{LR}	Shear modulus on combined radial and longitudinal surfaces
G_{23}	G_{RT}	Shear modulus on combined radial and tangential surfaces

Table 9
Wood elasticity parameters

E_L (MPa)	E_R (MPa)	E_T (MPa)	μ_{RT}	μ_{LR}	μ_{LT}	G_{LT} (MPa)	G_{LR} (MPa)	G_{RT} (MPa)
11319	1131.9	565.95	0.63	0.27	0.43	679.14	849.93	203.74

The simulation of the mixed connection of epoxy resin glue and self-tapping screws between the thin-walled beam flange and the wood plate is the key to the simulation analysis of the thin-walled steel-wood beam. From the test phenomenon of the combined beam, it can be seen that there is a slip between the thin-walled beam flange and the wood plate in the descending section of the load-displacement curve of the combined beam. In the late loading period, a large separation between the two materials of the combined beam occurs, and the self-tapping screws show a shear tilt performance.

5.2. Finite element model validation

The simulation of the combined beams adopts the displacement loading method, which sets a collection of reference points in the span of the specimen. Then set the course outputs of the corresponding loads and displacements to ultimately obtain the term load-deflection curves of each finite element model. Numerical simulation of seven combined beams is carried out by comparing the mid-span load-deflection curves of numerical analysis data and test information.

The physical significance of each parameter of wood material properties is shown in Table 8. The definition of each parameter is clarified in Table 9. The calculation method of the wood plastic yield strength coefficient is shown in Eq. (8):

$$R_{ij} = \begin{Bmatrix} \sigma_{ij} / \sigma_0 (i = j) \\ \sigma_{ij} / \tau_0 (i \neq j) \end{Bmatrix} \tag{8}$$

Material plasticity is defined with reference to yield stress σ_0, yield strength values for each material σ_{ij}. Moreover,the shear stress is τ^0, which is shown in Eq. (2):

$$\tau^0 = \sigma^0 / \sqrt{3} \tag{9}$$

From the combined view of the curves as shown in Fig. 15 (The horizontal axis is the span-to-span displacement of the combined beam specimen, and the vertical axis is the load applied to the combined beam.) In the elastic phase, the slope of the test and simulated values is in a linearly increasing direction. In the elastoplastic phase, the growth of the slope of the curves starts to slow down. It can be seen in the graphs of the two curves that the overall error of the two data is small. It shows that the model unit selection, the definition of material parameters, cohesive contact model used for the interface connection can be used in the simulation of this model. The finite element can well simulate the whole process of steel-wood combination beam bending deformation. The maximum load values of the finite element simulations are a little higher compared to the tests. The reason for this is that from the numerical simulation point of view. The wood properties in the numerical simulation are different from the actual wood. Secondly, from the experimental point of view, the original defects and dimensional defects of the wood were not taken into account, and the processing of the specimens also had an influence. However, the errors are within the allowable limits.

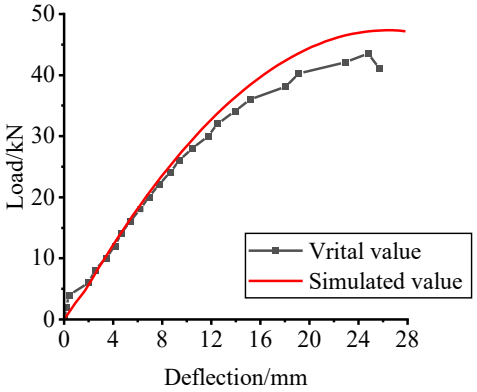

(a) L-1

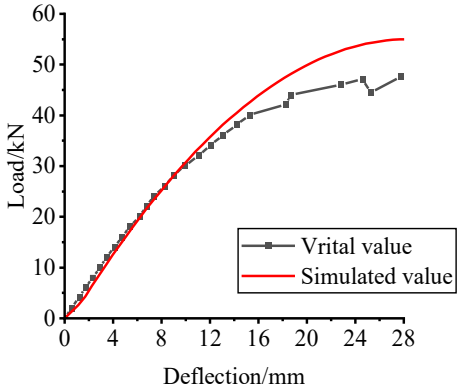

(b) L-2

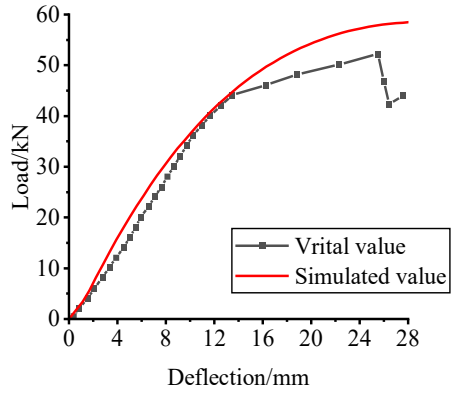

(c) L-3

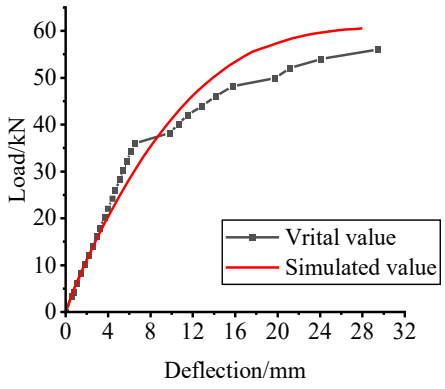

(d) L-4

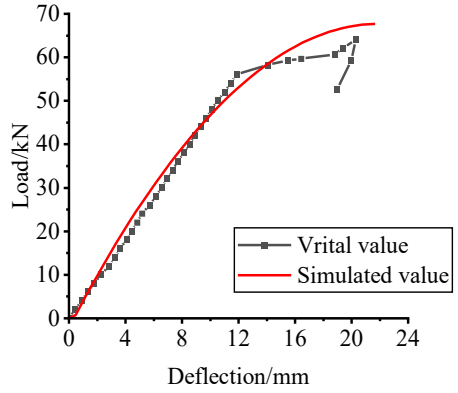

(e) L-5

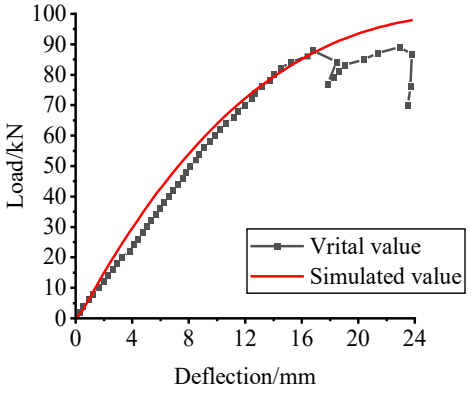

(f) L-6

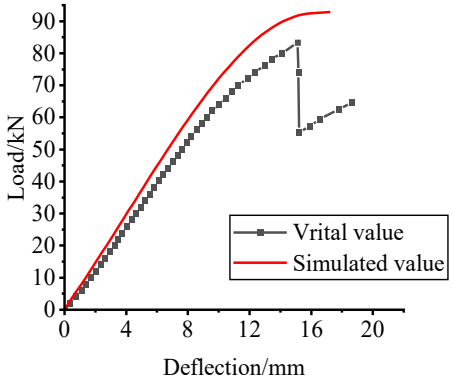

(g) L-7

Fig. 15 Comparison of experimental and numerical simulation load-deflection curves

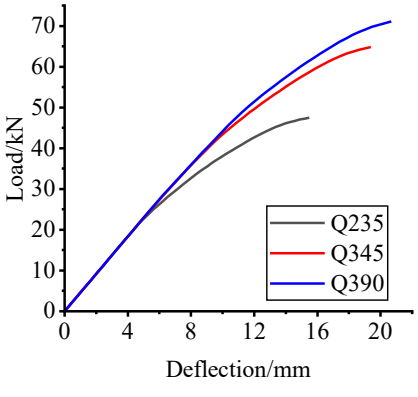

Fig. 16 Comparison of load-deflection curves at different yield strength spans

5.3. Parametric analysis of factors affecting the flexural performance of combined beams

5.3.1. Influence of steel yield strength

To study the effect of different yield strengths of steel on the bending performance of the combined beam. The Q235, Q345, and Q390 were selected as three kinds of steel with different yield strengths to simulate and analyze. Simulation of the three specifications of steel were taken as the yield strength of the yield strength value, modulus of elasticity, and Poisson's ratio are selected to take the value of the specification. As shown in Fig. 16, the load-displacement curves of the combined beams with different yield strengths of steel are compared.

As can be seen from the curve, the pre-loading period is characterized by an elastic trend of the three yield strengths of the combined beams in a line of linear development. The late loading of the combined beams to reach their respective yield strengths after the curve began showing non-linear development. With the increase of the yield strength, the load-carrying capacity of the combined beam also rises, when the steel specification changes

from Q235 to Q345. The load-carrying capacity of the specimen increases significantly, while when the steel specification changes from Q345 to Q390, the load-carrying capacity of the specimen increases by a small amount. Therefore, the increase in yield strength of steel is not obvious to improve the load-carrying capacity of the combined beam but will cause material waste.

5.3.2. Influence of the thickness of the combined beam flange planks

To study the influence of different thicknesses of flange planks on the bending performance of combined beams, Q235 specification, thickness of 1.5mm. And section size of 40mm×125mm×40mm were selected under the premise of the flange were 30mm, 35mm, and 40mm three plank thicknesses to simulate and analyze. As shown in Fig. 17, the load-displacement curves of the combined beams with different thicknesses of the flange planks are compared.

From the specimen load-deflection curves, it can be obtained that the maximum load-carrying capacity of the combined beam flange plank thickness increases from 30mm to 35mm and 40mm. Its maximum load-carrying capacity is also raised with the growth in the thickness of the flange plank. This is because of the increase in the thickness of the plank from 30mm to 35mm and 40mm when the specimen's cross-sectional stiffness changes, and there is a significant boost in the bending load-carrying capacity of the steel-wood beams.

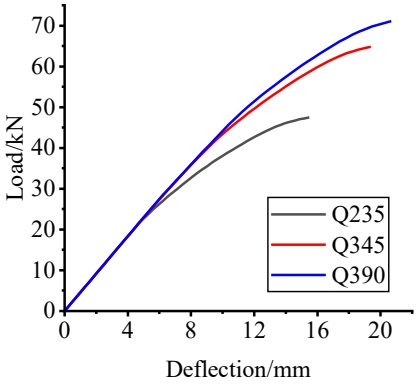

Fig. 17 Comparison of mid-span load-deflection curves for different thicknesses of wing planks

5.3.3. Combined beam thin-walled steel thickness effect

In order to study the combined beam, thin-walled steel thickness on the combined beam bending performance of the impact of different thicknesses. In the steel is selected Q235 specifications, the thickness of the wing edge board selection 30mm, and the steel size of 40mm × 125mm × 40mm under the premise of thin-walled steel thickness were selected 1.5mm, 2mm and 2.5mm thickness of the three kinds of simulation and analysis. As shown in Fig. 18, the load-displacement curves of combined beams with different thicknesses of thin-walled steel sections are compared. With the increase of the thickness of thin-walled steel sections in the combined beam, its flexural load capacity also has a large increase. The increase is about 10%.

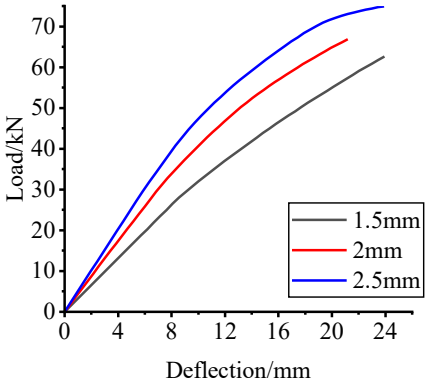

Fig. 18 Comparison of load-deflection curves at mid-span for different thicknesses of thin-walled sections

6. Conclusion

Since the strength of wood is much greater in the smooth grain than in the cross grain. The tensile strength is greater than the compressive strength. Steel has high strength, good plasticity and toughness properties, but thin-walled steel due to the thin wall thickness leads to its weak stability and other limitations of the material itself. A new thin wall H-section steel-wood composite beam member is proposed by combining the characteristics of the two materials, and seven different combination beams are tested for flexural performance. At the same time, ABAQUS finite element software is used to simulate the steel-wood combination beam and analyze its bending performance. The effects of the changes of the above factors on the bending capacity of steel-wood combination beams are analyzed. The following conclusions are obtained:

(1) The thin-walled steel profiles and wood are connected by epoxy resin glue and shear-resistant screws, which makes the combined beams have better integrity and give full play to the compressive and tensile properties of wood and thin-walled steel profiles. The stress process of the combined beam is mainly divided into three stages, i.e. elastic stage, elastic-plastic stage, and damage stage. In the elastic stage, the stiffness of the combined beam is large, and the steel and wood are jointly stressed. With the increase of load, when the combined beam reaches the elastic-plastic stage, the flange thin-walled steel appears local buckling; when the ultimate load is reached, the final damage phenomenon of the combined beam is the tensile bending damage of the lower flange board, and the combined beam damage mode is finally ductile damage.

(2) By analyzing the test data, it can be seen that under the same conditions. The change in the cross-section width of the combined beam has less influence on the bending capacity. The reduction of the shear screw spacing of the wing edge of the combined beam has no obvious effect on the load-carrying capacity but improves the connection performance of the interface. Changes in the height of the section of the combined beams had a significant effect on the load-carrying capacity. An increase in the thickness of the upper flange planks and an increase in the web height of the specimens resulting in a 52% and 45% increase in the load-carrying capacity, respectively. The change in the thickness of the flange planks had a greater effect on the load-carrying capacity than the change in the height of the webs. In the case where the thickness of the flange planks are 30mm, the increase in the thickness of the thin-walled steel sections results in a greater increase in the load-carrying capacity of the combined beams.

(3) A numerical simulation of seven combined beams was carried out using finite element software ABAQUS, and some factors affecting the bending performance of the combined beams, such as the yield strength of steel, thickness of the flange planks of the combined beams, and thickness of the thin-walled steel sections of the combined beams, were parametrically analyzed. The cohesive contact unit and modeling methods, such as load application and model boundary conditions are explored for simulation. The damage morphology and damage process of the steel-wood beams are verified more intuitively and the numerical simulation is compared with the test to verify its reasonableness.

Acknowledgments

This work is supported by the National Natural Science Foundation of Chi na (Grant No.52268029)and the Open Fund of Shock and Vibration of Engine ering Materials and Structures Key Laboratory of Sichuan Province (Grant No .20kfgk03).

Authorship contribution statement

Chang Wu: Conceptualization, Data curation, Methodology, Software, Visualization, Writing - original draft, Writing - review & editing.

Dongdong Ma: Investigation, Writing - review & editing, Validation.

Zhijiang Zhao: Writing - review & editing, Validation.

Yegong xu: Supervision, Investigation, Validation.

Renjun Fang: Software, Investigation, Methodology.

Conflict of interest statement

We declare that we have no financial and personal relationships with other people or organizations that can inappropriately influence our work.

References

[1] T. Chen, Z. Chen, J. Liu, Bending properties of cold-formed thin-walled steel/fast-growing timber composite I-beams, Forests, 15(5), 2024.

[2] Szewczak, Ilona, Rozylo, Influence of mechanical properties of steel and CFRP tapes on the

effectiveness of strengthening thin-walled beams, Materials, 14(9), 2380, 2021.
[3] A. M Guzman, V. A Roldan, Equivalent properties for analysis as beam-column of steel spatial lattices of rectangular cross-section, Adv. Steel Constr., 17(2), 95-103, 2021.
[4] S. Yan, Rasmussen Kim J. R., L. Jiang, Experimental evaluation of the full-range behaviour of steel beam-to-column connections, Adv. Steel Constr., 16(1), 77-84, 2020.
[5] L. Tian, Z. Li, M. Yang, Lateral torsional buckling strength of steel I-beams within preflexed beams in pre-bending stage, Adv. Steel Constr., ,16(1), 47-54, 2020.
[6] H. Yang, H. Guo, Y. Wang, H. Jiang, Research on the shear performance of cold-formed thin-walled steel-glued laminated wood composite beams, Buildings, 13(12), 2023.
[7] E. McConnell, D. McPolin , S. Taylor, Post-tensioning of glulam timber with steel tendons, Constr. Build Mater. 73, 426-433, 2014.
[8] C. Marco, V. M. Chandra, E. Vikki, Local FRP reinforcement of existing timber beams, Compos. Struct. 258, 2021.
[9] J. Aidas, V. Juozas, Analysis of the transfer, flexural bond and anchorage lengths of pretensioned FRP reinforcement based on Eurocode, Compos. Struct. 327, 2024.
[10] H. Zhe, W. Yang, Y. Zhang, K. Zhao, Z. Dong, Flexural performance of FRP-SWSSC-steel composite beams: Experimental and analytical investigation, Eng. Struct. 306, 2024.
[11] Szewczak, Ilona, Rozylo, Impact of adhesive layer thickness on the behavior of reinforcing thin-walled sigma-type steel beams with CFRP tapes, Materials, 15(3), 1250, 2022.
[12] M. He, Y. Wang, Z. Li, An experimental and analytical study on the bending performance of CFRP-reinforced glulam beams, Front. Mater. 8, 2022.
[13] A. Hassanieh, H. Valipour, M. Bradford, Composite connections between CLT slab and steel beam: Experiments and empirical models, J. Constr. Steel Res. 138, 823-836, 2017.
[14] L. Wang, J. Lyu, J. Zhao, Experimental investigation of the shear characteristics of steel-to-timber composite joints with inclined self-tapping screws, Eng. Struct. 215, 2020.
[15] A. A. Chiniforush, H. R. Valipour, A. Akbarnezhad , Long-term coupled analysis of steel-timber composite (STC) beams, Constr. Build Mater. 278, 2021.
[16] Y. Zhao, Y. Yuan, C. Wang, Experimental and finite element analysis of flexural performance of steel-timber composite beams connected by hybrid-anchored screws, Eng. Struct. 292, 2023.
[17] X. Song, L. Zhao, Y. Liu, Experimental and nonlinear analytical of the flexural performance of timber-filled steel tubular composite beam, Eng. Struct. 301, 2024.
[18] G. Li, W. Zhang, X. Li, B Yang, Flexural behavior of cold-formed thin-walled steel-glulam composite beams, Wood Mater. Sci. Eng. 18(1), 289-302, 2023.
[19] S. Duan, W. Zhou, X. Liu, J. Yuan, Experimental study on the bending behavior of steel-wood composite beams, Adv. Civ. Eng. 2021, 2021.
[20] R. Yang, H. Li, R. Lorenzo, Mechanical behavior of steel timber composite shear connections, Constr. Build Mater. 258, 2020.
[21] T Chen, Z Chen, J Liu, A Zhang, Benging properties of cold-formed thin-wall steel/fast-growing timber composite I-beams, Forests, 15(5), 857, 2024.
[22] S Duan, W Zhou, X Liu, J Yuan, Z Wang, Experimental study on the bending behavior of steel-wood composite beams, Adv. Civ. Eng., 2021(1), 2021.
[23] Li, Y. Qiu, Young, Ben, Structural performance of cold-formed steel built-up section beams under non-uniform bending, J. Constr. Steel Res. ,189, 2022.
[24] C. Wu, J. Duan, Z. Yang, Z. Zhao, Y. Xu, A novel rectangular-section combined beam of welded thin-walled H-shape steel/camphor pine wood: The bending performance study, Sustainability, 15(9), 7450-7450, 2023.
[25] X. Zhao, L.Wei, D.Wen, Bending response and energy absorption of sandwich beams with novel auxetic honeycomb core, Eng. Struct. ,247, 2021.
[26] W. Gu, H. Liu, Y. Dong, Experimental study on the flexural properties of concrete beams reinforced with Hybrid steel/Fiber-Belt-Bars, Materials, 15(10), 3505, 2022.
[27] L. Zhang, J. Zhang, G. Chen, G. Lin, Flexural behavior of hybrid FRP-recycled aggregate concrete-steel hollow beams, J. Constr. Steel Res. 200, 2023.
[28] U. Hilal, B. Agron, D. Nihat, I. H. Ozgur, S. Cevde, Modulus of elasticity and flexural behavior of glulam beams reinforced with steel mesh in different mesh openings, Materials, 16(12)4307, 2023.
[29] B.C. Alberto, V. S. D. Brother, P. K. Augusto, Flexural and shear behavior of steel-UHPC composite beams: a review, Eng. Struct. 293, 2023.
[30] S. Yuka, N. Yukihiro, U. Akikazu, Dissimilar materials bonding using epoxy monolith, ACS omega 3(7), 7532-7541, 2018.
[31] Y. Li, C. Li, J. He, Y. Gao, Z. Hu, Effect of functionalized nano-SiO2 addition on bond behavior of adhesively bonded CFRP-steel double-lap joint, Constr. Build Mater. 244, 2020.
[32] B. J. A. Tadeu, G. F. J. F. Branco, Shear tests of steel plates epoxy-bonded to concrete under temperature, J. Matre. Civil Eng. 12(1), 74-80, 2000.
[33] Feng ,H. Qiang, L. Ye, Definition and discussion of "yield point" of materials, components and structures. Engineering Mechanics, 34(3), 36-46, 2017, [in Chinese].
[34] Ministry of Construction of the People's Republic of China, Steel structure design code GB50017-2017, China Planning Press, 2017, [in Chinese].
[35] Ministry of Construction of the People's Republic of China, Wood structure design code GB50005-2017, China Construction Industry Press, 2017, [in Chinese].